Semiconductor Characterization Techniques

18

18.1 Introduction

Semiconductor characterization techniques are used in order to gain knowledge on the physical properties of a semiconductor crystal. The process is similar to decoding the DNA sequence of a living organism as it involves understanding the nanoscale structure of the crystal, i.e., its atoms, electrons, structures, and interactions with the surrounding environment. The knowledge gained from the characterization process is essential in determining whether the semiconductor crystal probed is suitable for a particular device component with certain functionalities.

Semiconductor characterization is generally initiated immediately after the synthesis of a crystal. We can distinguish three types of characterization techniques: structural, optical, and electrical. In this chapter, we will briefly review the most common of these semiconductor characterization techniques. The discussion and examples will be primarily directed toward semiconductor thin films, although most of the same techniques can be readily used for bulk crystals as well.

18.2 Structural Characterization Techniques

18.2.1 X-ray Diffraction

X-ray diffraction employs electromagnetic waves with a wavelength on the order of one angstrom. Since wave diffraction occurs when the dimensions of the diffracting object are of the same order of magnitude as the wavelength of the incident wave, X-rays are ideally suited to probe crystal lattice structures.

X-ray diffraction of semiconductor thin films is generally carried out in a diffractometer. The source of the X-rays is called an X-ray tube (Fig. 18.1) and consists of a water-cooled copper target onto which an accelerated electron beam (up to a few 10's of keV) is impinging inside a vacuum tube. Because of the bremsstrahlung

M. Razeghi, *Fundamentals of Solid State Engineering*,
https://doi.org/10.1007/978-3-319-75708-7_18

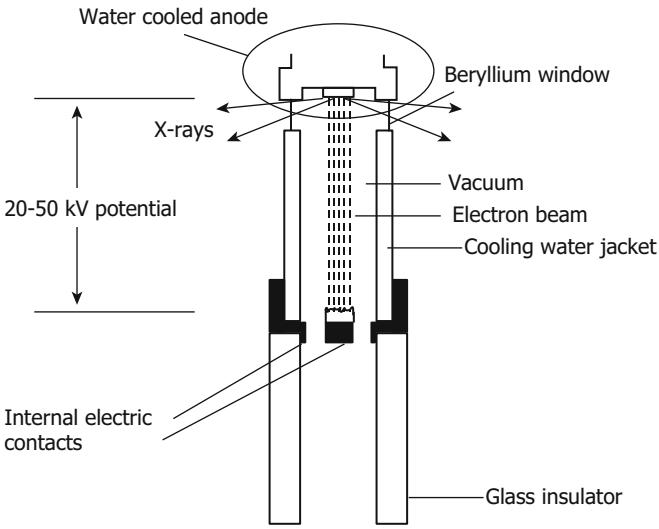

Fig. 18.1 Schematic diagram of an X-ray tube

effect, X-rays are emitted with wavelengths that are characteristic of the copper element. Bremsstrahlung is the original German name for the effect of generation of X-rays via electron deceleration through its interaction with the Coulomb field of the nucleus (of copper, in this case). Through these inelastic interactions, X-rays are emitted which can have energies as high as the beam energy. These X-rays are then filtered and collimated into a beam through the use of a monochromator consisting of nearly perfect silicon crystals placed at specifically chosen angles to permit reflection of the X-rays.

Diffracted waves from different atoms can interfere with each other, and the resultant intensity distribution is strongly modulated by this interaction. If the atoms are arranged in a periodic fashion, as in crystals, the diffracted waves will consist of sharp interference maxima (peaks) with the same symmetry as in the distribution of atoms. Measuring the diffraction pattern therefore allows us to deduce the distribution of atoms in a material.

The peaks in an X-ray diffraction pattern are directly related to the atomic distances. For a given set of lattice planes with an interplane distance d, the condition for a diffraction (peak) to occur can be found using Bragg's law:

$$2d \sin\theta = n\lambda \tag{18.1}$$

where θ is the incident angle, λ is the wavelength of the X-ray, and n is an integer representing the order of the diffraction peak. This process is shown schematically in Fig. 18.2.

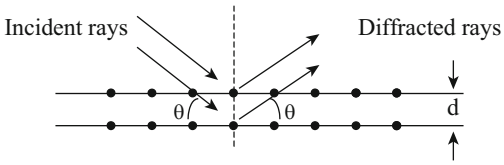

Fig. 18.2 Schematic of diffraction of X-rays by a crystal

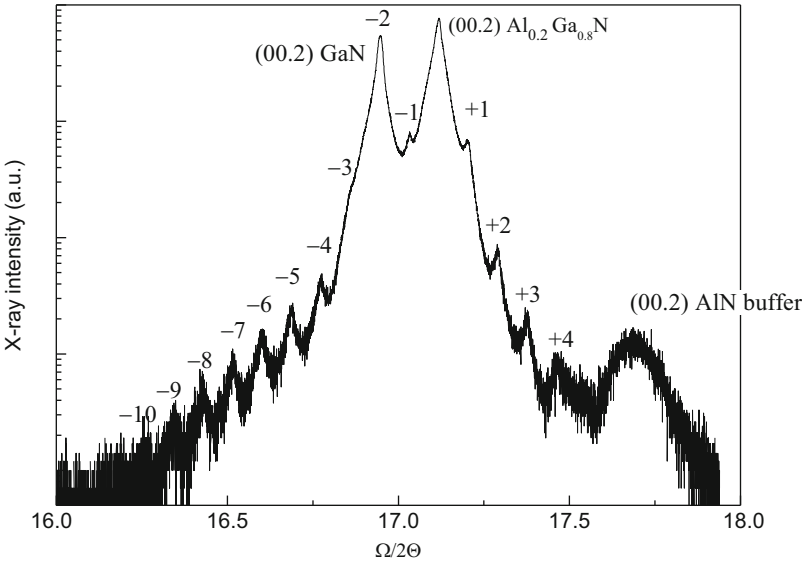

Fig. 18.3 X-ray curve of an $Al_{0.2}Ga_{0.8}N$/GaN superlattice grown on GaN/AlN buffer layer. The individual $Al_{0.2}Ga_{0.8}N$, GaN, and AlN peaks as well as the superlattice satellite peaks are clearly discernible on the graph

Figure 18.3 shows an X-ray diffraction curve of an $Al_{0.2}Ga_{0.8}N$/GaN superlattice structure grown on a GaN template layer. X-ray diffraction measurements on semiconductors can yield useful information such as:

- Lattice constants: The mismatch between the epilayer and the substrate perpendicular to the growth plane can be determined, which is also indicative of strain and stress.
- Rocking curve: The width of the X-ray rocking curve, also called full width at half maximum (FWHM) in units of arcsec or arcmin, is inversely related to the number of dislocations in the epilayer. Therefore this measurement can be used as a measure of the film quality.
- Thickness and quality of superlattices: Thickness of the various layers in multilayer structures like superlattices can be determined by the distance between the satellite peaks appearing on the sides of the main peak. Also the intensity and number of satellite peaks are measures of the film quality.

18.2.2 Electron Microscopy

Scanning Electron Microscopy

A scanning electron microscope (SEM) is probably the most widely used semiconductor characterization instrument. A schematic of a typical SEM system is shown in Fig. 18.4. Electrons are emitted from a tungsten cathode either thermionically or via field emission and are focused by two successive condenser lenses into a very narrow beam. Two pairs of coils deflect the beam over a rectangular area of the specimen surface. Upon impinging on the specimen, the primary electrons transfer their energy inelastically to other atomic electrons and to the lattice. Through many random scattering processes, some electrons manage to leave the surface to be collected by a detector facing the specimen. Usually these are the secondary electrons, originated from a depth of no larger than several angstroms, that are collected by the detector. A photomultiplier tube (PMT) amplifier is used to amplify the signal, and the output serves to modulate the intensity of a cathode ray tube (CRT). Research-quality SEMs are generally able to produce images with a resolution of ~50 Å.

SEM not only can provide images of the surface but also, by rotating the sample, one can obtain information about the thickness of various layers in the structure (cross-sectional SEM). Figure 18.5a illustrates a bird's eye view image of a surface of a "nanopillar" sample, while Fig. 18.5b displays the cross section of a multilayer semiconductor structure.

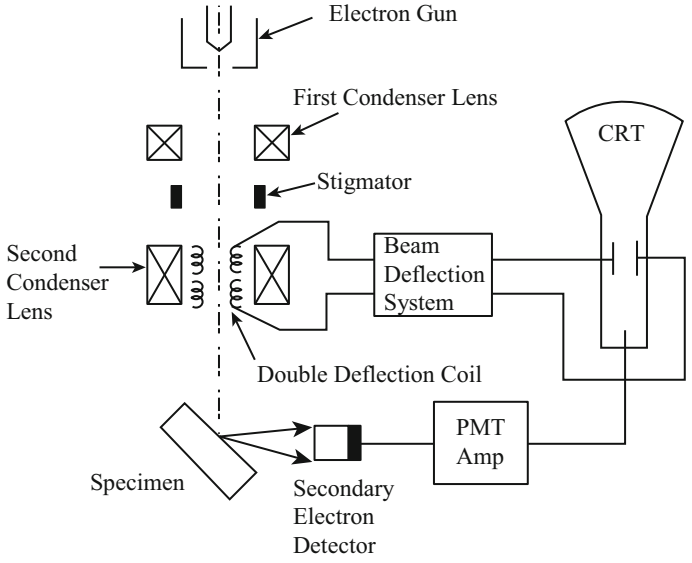

Fig. 18.4 Schematic of a scanning electron microscope

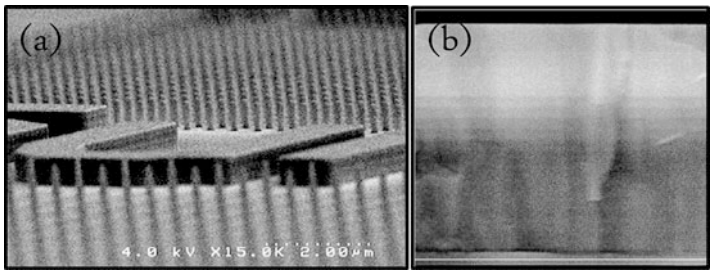

Fig. 18.5 (**a**) Bird's eye view of the surface of a nanopillar sample and (**b**) cross-sectional SEM image of a multilayer semiconductor structure

Transmission Electron Microscopy

Transmission electron microscopy (TEM) is a complex characterization technique that takes advantage of electron diffraction to give the user valuable information regarding the crystallography of the films and, in the image mode, provide high-resolution images of both plain-view and cross-sectional view of the films. A variety of useful information, such as defect structures, structure of grain boundaries, phase identification, crystallographic orientation, quality of the interfaces, etc., can be obtained using this technique.

Figure 18.6 shows the two basic modes of operation of TEM, image mode and diffraction mode. Electrons are thermionically emitted from the gun and are accelerated to high voltages (in excess of 100 keV). A condenser lens section projects the electron beam onto the specimen. Two types of scattering can occur when electrons hit the specimen: elastic scattering results in no loss of energy, while inelastic scattering involves some energy loss. Diffraction patterns can be obtained from elastically scattered electrons, while inelastically scattered electrons give rise to a spatial variation in the intensity of the transmitted beam. Inelastic interactions between the electron beam and the specimen at grain boundaries, dislocations, defect sites, density variations, etc. are the cause of inelastic scattering. Figure 18.5 shows a high-resolution lattice image of the AlN/Al_2O_3 interface. Dislocations can be identified when any of the atomic planes terminates (Fig. 18.7).

TEM is capable of producing high magnifications, due to the small effective wavelengths that are used. Recalling de Broglie's relation from (Eq. 3.3):

$$\lambda = \frac{h}{p} \tag{18.2}$$

As mentioned above, electrons are accelerated to very high energies. If we let this potential energy, eV, equal the kinetic energy of the electrons:

$$\mathrm{eV} = \frac{m_0 v^2}{2} \tag{18.3}$$

the momentum of an electron can be written as:

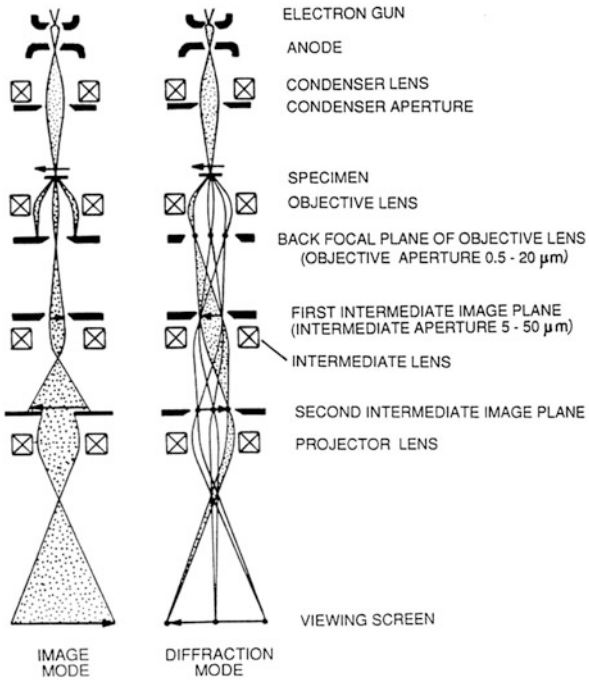

Fig. 18.6 Schematic of the TEM in imaging and diffraction modes. (Reprinted from Thomas G, Goringe MJ Transmission electron microscopy of materials, Fig. 6.10. Copyright 1979 by John Wiley and Sons. Reprinted with permission of CBLS)

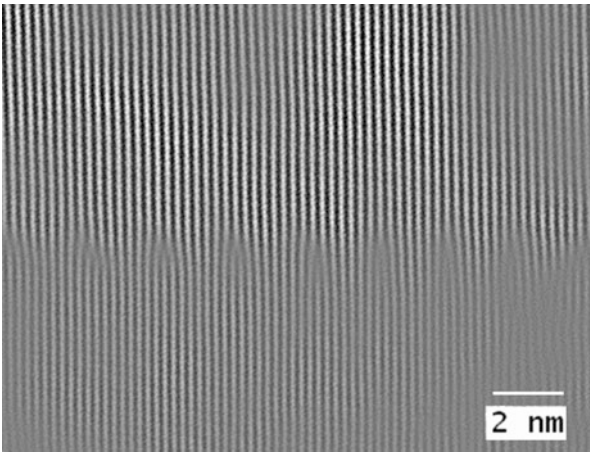

Fig. 18.7 High-resolution TEM image of the interface of AlN and sapphire (Al_2O_3). One misfit dislocation generates when an atomic plane ends

$$p = m_0 v \tag{18.4}$$

Therefore, the wavelength of the electrons, from the above three equations, can be expressed as:

$$\lambda = \frac{h}{\sqrt{2m_0 \mathrm{eV}}} \tag{18.5}$$

For instance, if the acceleration energy of 100 keV is applied, the wavelength will be as small as 0.0386 Å. It should be noted that at such high energies, the velocity of the electrons becomes comparable with the velocity of light. Therefore, in order to have a more accurate evaluation of the wavelength, relativistic effects have to be considered. The modified expression is:

$$\lambda = \frac{h}{\sqrt{2m_0 \mathrm{eV}\left(1 + \frac{\mathrm{eV}}{2m_0 c^2}\right)}} \tag{18.6}$$

For example, with an acceleration voltage of 1 MV, the nonrelativistic wavelength is 0.0122 Å, while the relativistic value is only 0.0087 Å (Williams and Carter 1996).

18.2.3 Energy Dispersive Analysis Using X-rays (EDX)

In EDX an electron from an outer shell of an atom (e.g., the 2*s* shell) lowers its energy to fill the hole in a lower shell (e.g., the 1*s* shell) which results in the emission of an X-ray. These emitted X-rays are characteristic of the particular atom undergoing emission. Therefore, by looking at the X-ray spectral lines of an atom, one could identify that specific atom.

Majority of EDX systems are interfaced to SEM, where they use the same electron beam source to excite X-rays from the specimen under study. A cooled Si (Li) detector (lithium drifted silicon detector) is used to detect X-rays. An emitted X-ray from a specimen generates a photoelectron upon interception by the detector. This photoelectron in turn generates an electron-hole pair. The number of electron-hole pairs, or equivalently the amplitude of the generated voltage pulse, is proportional to the incident photon energy. After amplifying, sorting, counting, and storing the pulses within a range of voltages (energies), the final spectrum will be plotted. Figure 18.8 shows an example of an EDX plot.

18.2.4 Auger Electron Spectroscopy (AES)

The AES technique takes advantage of the Auger transitions that were introduced in Chap. 8. In an Auger process, three electron levels are involved: an electron from an outer level lowers its energy to fill a hole. Instead of generating a photon, this process can result in the ejection of an electron from a third level. The electron that leaves the atom is called the Auger electron. Similar to EDX, the particular atom under test can be identified by looking at the Auger spectral lines.

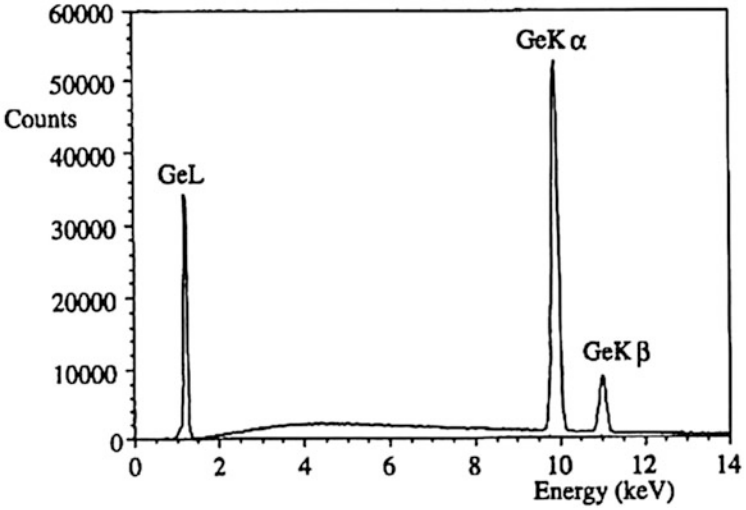

Fig. 18.8 An example of an EDX measurement. Multiple lines of Ge emission correspond to the various electron energy transitions. (Reprinted with permission of Springer Science and Business Media. Williams DB, Carter CB Transmission electron microscopy, p. 557, Fig. 32.2. Copyright 1996 Plenum Press, New York)

A typical Auger spectrometer is kept under ultrahigh vacuum (10^{-10} Torr level) to avoid contaminations. A focused electron beam source of ~2 keV in energy is scanned over the sample area under test. The emitted Auger electrons are then analyzed by an analyzer. The Auger peaks are barely distinguishable above the background signal; therefore, in order to accentuate the energy and magnitude of these peaks, the differentiated signal is generally plotted, as shown in Fig. 18.9.

18.2.5 X-ray Photoelectron Spectroscopy (XPS)

In the XPS technique, low-energy X-rays are used as a source rather than electrons in the case of EDX and AES. Electrons are ejected when the photon is absorbed via the photoelectric effect. In this case the energy of the ejected electron can be written as:

$$E_{\mathrm{KE}} = h\upsilon - E_{\mathrm{BE}} \tag{18.7}$$

where E_{KE} is the energy of the ejected electron, hυ is the energy of the incident photon, and E_{BE} is the energy of the involved bound electron state. By measuring the photoelectron energy, it will be possible to identify the particular atom, since the values of binding energy are element specific. An example of an XPS spectrum (for silver (Ag)) is shown in Fig. 18.10. It should be noted that for multicomponent samples the intensities of the peaks are proportional to the concentration of the element within the sampled region.

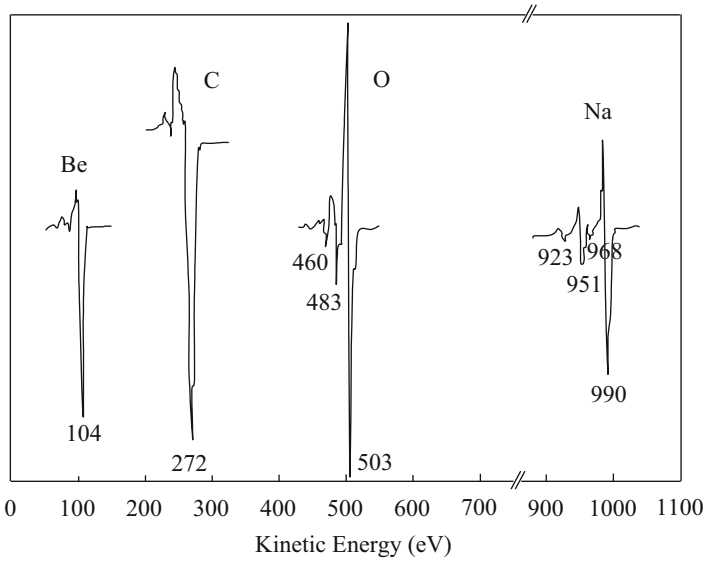

Fig. 18.9 Auger electron spectra of various elements

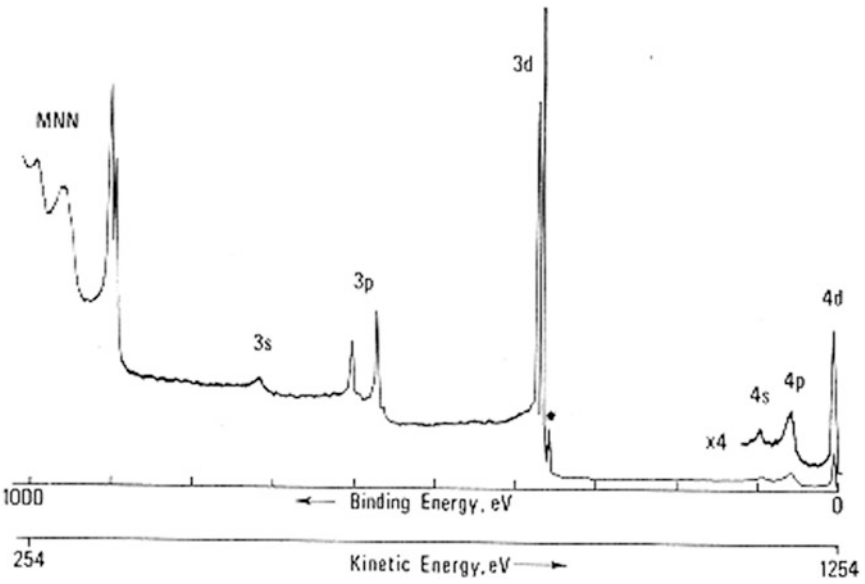

Fig. 18.10 An XPS spectrum from a silver sample (Reproduced with permission. Briggs D, Seah MP Practical surface analysis: by Auger and X-ray photoelectron spectroscopy, p. 112, Fig. 3.16. Copyright 1983 John Wiley & Sons Limited)

18.2.6 Secondary-Ion Mass Spectroscopy (SIMS)

SIMS is a technique used to identify and quantify various types of atoms on the surface or inside a solid sample. In SIMS the material is bombarded by a beam of high-energy ions (1~30 keV) resulting in the ejection or sputtering of atoms from the material. A small percentage of these ejected atoms leave as either positively or negatively charged ions, which are referred to as "secondary ions."

These sputtered secondary ions are then collected and analyzed by a mass-to-charge spectrometer. Elements are identified through their atomic mass values, while their concentration is determined by counting the number of corresponding secondary ions.

The sensitivity of a SIMS measurement is dependent upon the yield of secondary-ion sputtering, which in turn depends on the material under study, the specimen's crystallographic orientation, and the nature, energy, and incidence angle of the primary beam of ions. The proper choice of primary ion beam is therefore important in enhancing the sensitivity of SIMS. O_2^- atoms are usually used for sputtering electropositive elements or those with low ionization potentials such as Na, B, and Al. On the other hand, Cs^+ atoms are better at sputtering negative ions from electronegative elements such as C, O, and As. The detection limit of SIMS is severely reduced with improper selection of the ion beam. Liquid metal ion sources are used for high-resolution measurements, since they can provide smaller beam diameters.

Two types of SIMS are usually considered: "static" SIMS works with low-energy ion sources (0.5–3 keV) which result in low sputter rates (in units of monolayers per second). This mode of operation is suitable for surface analysis, since it will take a long time for the surface to be modified by ion bombardment. "Dynamic" SIMS, on the other hand, uses high-energy ion beams (higher than 3 keV) which results in high sputter rates. This mode of operation is suited for depth profile analysis of the sample under test. Figure 18.11 shows a SIMS depth profile of a GaN sample showing its concentration of impurities (oxygen, carbon, silicon) using Cs^+ bombardment.

18.2.7 Rutherford Backscattering (RBS)

In the RBS technique, very high-energy beams (in the MeV range) of low mass ions (He, C, N, etc.) are accelerated, collimated, and focused upon the sample under test. These high-energy beams have the ability to penetrate deep into the sample (several microns). Such beams cause little sputtering of the surface atoms. Sometimes they penetrate the atomic electron cloud shield and collide with the nuclei of the target atoms. The result is an elastic scattering from the Coulomb repulsion between ion and nucleus, known as Rutherford scattering.

From energy and momentum conservation laws, we know that if an incident ion of mass M_0 and energy E_0 hits a surface atom of mass M, the elastic collision will cause the ion to have an energy E_1 afterward given by Ohring (1992):

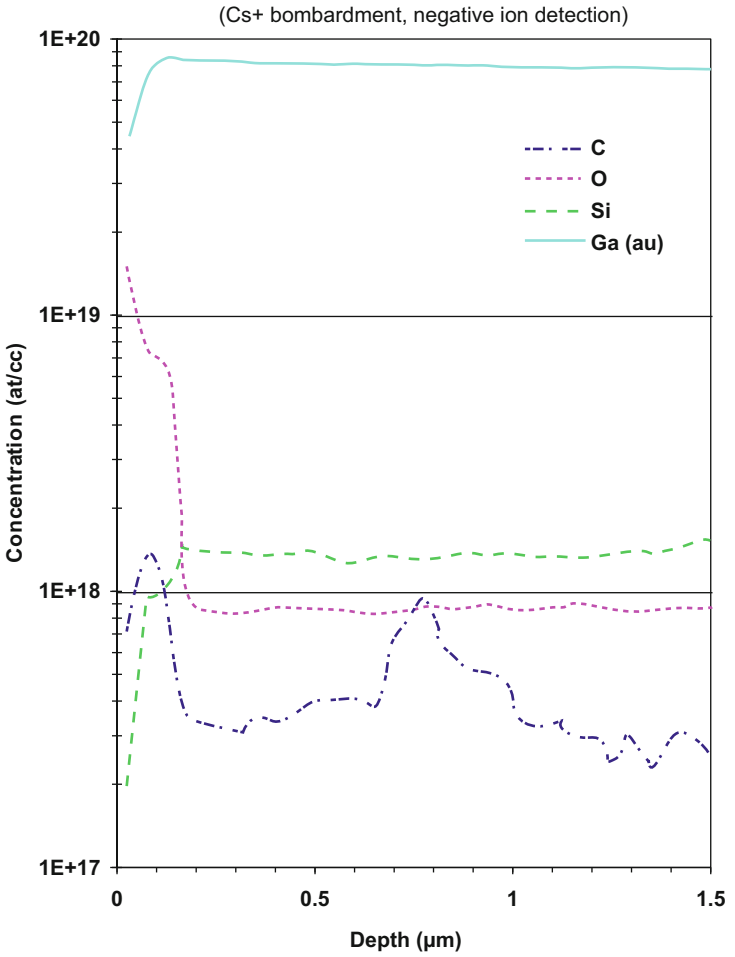

Fig. 18.11 A SIMS depth profile showing the concentration of impurities in a GaN sample. The impact energy was 15.5 keV at oblique incidence and the detected area was 33 μm in diameter

$$E_1 = \left\{ \frac{\left(M^2 - M_0^2 \sin^2\theta\right)^{1/2} + M_0 \cos\theta}{M_0 + M} \right\}^2 E_0 \tag{18.8}$$

where θ is the scattering angle. At a fixed value of M_0 and θ, E_1 depends only on the atomic weight of the target atom. Therefore, E_1 will be different for different targets, and by detecting this energy, one can distinguish between different atoms. This technique can be applied to multilayer samples as well. In this case not only the energy of the scattered beam but its intensity will also be affected by numerous scatterings inside the sample. In this case, top layers will have higher intensity scattered beams than the underlying layers.

18.2.8 Scanning Probe Microscopy (SPM)

Scanning probe microscopy (SPM) is a useful method for the study of the surface morphology. This method employs the concept of scanning an extremely sharp tip (3~50 nm radius of curvature) across the object surface. The tip is mounted on a flexible cantilever, allowing the tip to follow the surface profile (Fig. 18.12). When the tip moves in the proximity of the object under investigation, forces of interaction between the tip and the surface influence the movement of the cantilever. These movements are detected by selective sensors.

There are three major types of SPM:

- Atomic force microscopy (AFM) measures the interaction force between the tip and the surface. The tip may be dragged across the surface or may vibrate as it moves. The interaction force will depend on the nature of the sample, the probe tip, and the distance between them.
- Scanning tunneling microscopy (STM) measures a weak electrical current flowing between tip and sample as they are held a very short distance apart.
- Near-field scanning optical microscopy (NSOM) scans a very small light source very close to the sample. Detection of this light energy forms the image. NSOM can provide resolution below that of the conventional light microscope.

Essential to the system is a piezoelectric tube (Fig. 18.13). It consists of a piezo material inserted inside a hollow tube. Pairs of electrodes on the inner and outer walls are placed on either side of the tube. When suitable voltage differences are

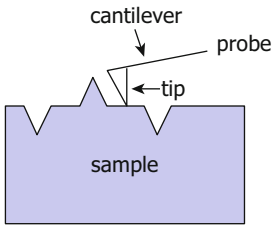

Fig. 18.12 Schematic of an AFM tip scanning over the surface of a sample

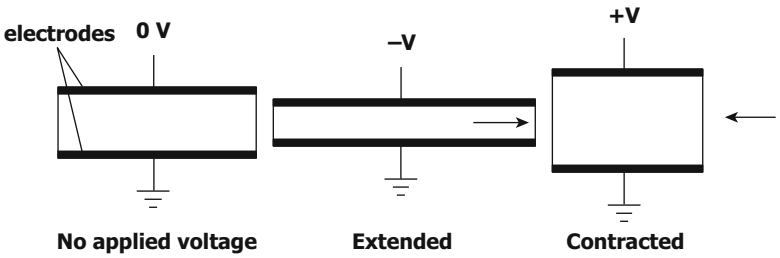

Fig. 18.13 Reaction of a piezo material to applied bias

applied to these electrodes, one side of the tube expands, and the other side contracts. This results in a bending of the tube; hence if one end is fixed, the other end moves, resulting in the scanning motion. Two sets of electrodes, 90 degrees apart, allow motion in the *x*-*y* plane. A further pair of electrodes extending around the entire circumference of the tube cause an entire section of the tube to expand or contract, resulting in the free end of the tube moving parallel to the tube axis (the *z*-axis). The combination of all three sets of electrodes allows movement of the free end of the tube to be controlled very precisely in all three axes. For surface mapping applications, the feedback provided by the probe and detector is used to keep the probe at a constant distance from the surface (*z*-direction), while it is free to move across the surface (*x*- and *y*-directions). This is accomplished by applying a voltage to the piezoelectric tube. This voltage is proportional to the probe's movement in *z*-direction which is then used to generate the surface topology.

The AFM is capable of reconstructing the surface morphology of the materials with atomic scale precision. An example of a three-dimensional image of the surface of InAs quantum dots grown on GaAs/InP is shown in Fig. 18.14.

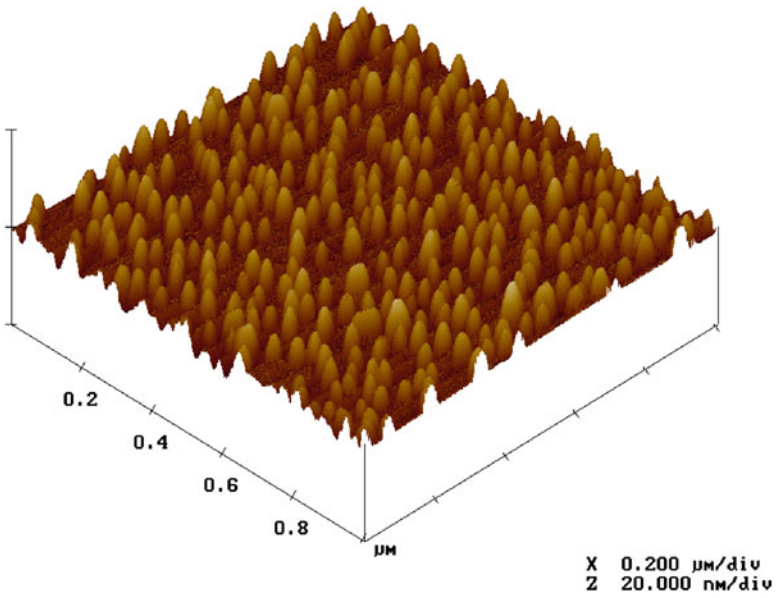

Fig. 18.14 A 3D AFM image of the surface of a sample consisting of InAs quantum dots grown on top of a GaAs/InP substrate

18.3 Optical Characterization Techniques

18.3.1 Photoluminescence Spectroscopy

Photoluminescence (PL) spectroscopy is a nondestructive method of probing the electrical properties of materials. Light is focused onto the sample where it is absorbed in a process called "photoexcitation." As a result of the excess energy caused by photoexcitation, electrons jump to permissible excited states. When these electrons move back to their equilibrium states, the excess energy is released through emission of light with energy equal to the energy difference between the equilibrium and excited states. This emitted light is then focused and collected by a photon detector through a spectrometer. A PL spectrum for an AlGaN sample is shown in Fig. 18.15. Many useful information can be extracted out of PL spectra:

- Bandgap determination: The most common radiative transition in semiconductors is between the states in the conduction and valence bands, which equals to the energy gap of the semiconductor.
- Impurity levels and defect detection: Radiative transitions in semiconductors involve localized defect levels. The photoluminescence energy associated with these levels can be used to identify specific defects.
- Recombination mechanisms: When the electrons return to their equilibrium states, also known as "recombination," both radiative and nonradiative processes can occur. The intensity of the PL peak and its dependence on the level of photoexcitation and temperature is directly related to the dominant recombination process.

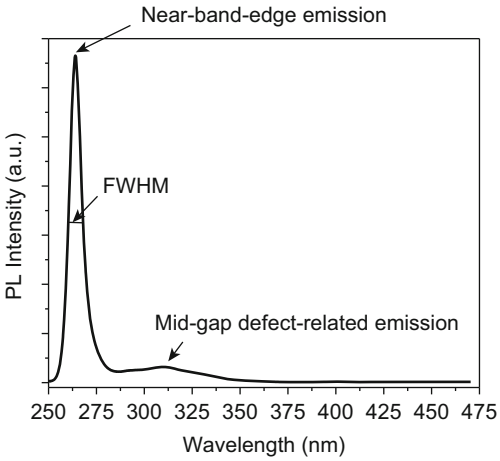

Fig. 18.15 Photoluminescence spectrum of an AlGaN sample. Shown on the graph are the near-band-edge emission peak and a defect-related emission peak

- Material quality: The intensity and the line width (FWHM) of a PL spectrum are representative of the quality of the material. Additionally, the presence of defect-related peaks is indicative of imperfections in the epitaxial layer.

18.3.2 Cathodoluminescence Spectroscopy

Cathodoluminescence (CL) spectroscopy is similar to PL in almost every aspect, except for the radiation source. In CL, electrons are used to excite the sample instead of photons in the PL case. The electron source can be the focused beam used in SEMs. Similar to PL spectra, CL spectra contain many useful information such as the ones listed in the previous subsection.

18.3.3 Reflectance Measurement

Any light incident upon any medium undergoes partial transmission, absorption, and reflection. The reflected part of the light can be collected and measured against a reference sample, typically a near-ideal mirror, to obtain the reflectivity. Reflectance is defined as the ratio of the reflected to incident light, given by Fresnel equations Eq. (10.22) as:

$$R = \left|\frac{E_\mathrm{r}}{E_\mathrm{i}}\right|^2 = \left(\frac{\bar{n}-1}{\bar{n}+1}\right)^2 \tag{18.9}$$

where E_r and E_i are the energy of the reflected and incident light, respectively, and $\bar{n}$ is the refractive index of the medium.

18.3.4 Absorbance Measurement

A visible/UV light beam is incident upon the sample under study and a reference sample simultaneously. The transmitted light out of the other face of the sample is collected by a photodetector through a spectrometer, and its intensity relative to the reference sample is plotted as a function of wavelength. This way one can determine the transmittance or absorbance of the sample under study as a function of wavelength. This method is especially useful for obtaining the absorption edge (cutoff wavelength) associated with the material. The band-to-band absorption in a semiconductor (see Chap. 10) gives the following relationship between the absorption coefficient α (see Eq. 10.81), the light energy E, and the bandgap energy E_g:

$$\alpha \propto \sqrt{E - E_\mathrm{g}} \tag{18.10}$$

18.3.5 Ellipsometry

Ellipsometry measures the change in the polarization state of light reflected from the surface of a sample. The measured parameters are the amplitude ratio (tan Ψ) and the phase difference (Δ) of the two components of reflected light. These values are related to the ratio of Fresnel reflection coefficients, R_p and R_s, for p- and s-polarized light, respectively:

$$\tan(\Psi)e^{i\Delta} = \frac{R_p}{R_s} \tag{18.11}$$

This simple fundamental equation of ellipsometry relates refractive indices of the film, and the substrate, film thickness, and phase changes during reflection at the film interfaces.

In Fig. 18.16, a linearly polarized input beam is converted to an elliptically polarized reflected beam. For any angle of incidence greater than 0° and less than 90°, *p*-polarized and *s*-polarized lights will be reflected differently.

The ellipsometry apparatus can also be used to measure transmission and reflection of samples. In this mode, the transmission (T) and reflection (R) values are determined via:

$$T = \frac{I_t}{I_i} \text{ and } R = \frac{I_r}{I_i} \tag{18.12}$$

where I_i, I_t, and I_r are the intensities of the incident, transmitted, and reflected lights, respectively.

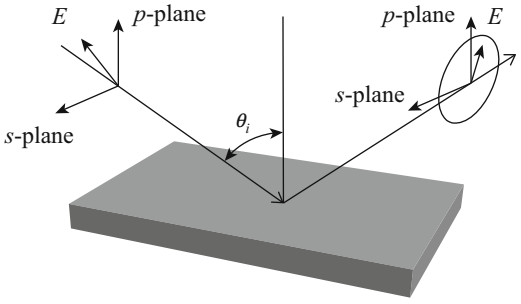

Fig. 18.16 Schematic of the geometry of an ellipsometry measurement. The coordinate system used to describe the ellipse of polarization is the p-s coordinate system. The s-direction is taken to be perpendicular to the direction of propagation and parallel to the sample surface. The p-direction is taken to be perpendicular to the direction of propagation and contained in the plane of incidence

18.3.6 Raman Spectroscopy

When photons are incident upon a medium, they get scattered either elastically (Rayleigh scattering) or inelastically (Raman scattering). In Rayleigh scattering, the energy of the emitted photon is the same as the incident photon. On the other hand, in Raman scattering, the energies of the scattered and incident photons are different. The energy change is depicted in Fig. 18.17, where an incoming photon either creates a phonon and is remitted at a lower energy (anti-Stokes scattering) or annihilates a phonon and is remitted at a higher energy (Stokes scattering). The inelastically scattered light can be collected, and information about the energy levels within the medium can be deduced from the energy change in the light.

A monochromatic light source, usually an argon ion laser, is used to excite the sample, and a spectrometer/PMT set is used to detect the scattered light. An example of a Raman spectrum is schematically shown in Fig. 18.18.

18.3.7 Fourier Transform Spectroscopy

A Fourier transform spectrometer is a Michelson interferometer with a movable mirror. By scanning the movable mirror over some distance, an interference pattern is produced that encodes the spectrum of the source (in fact, it turns out to be its

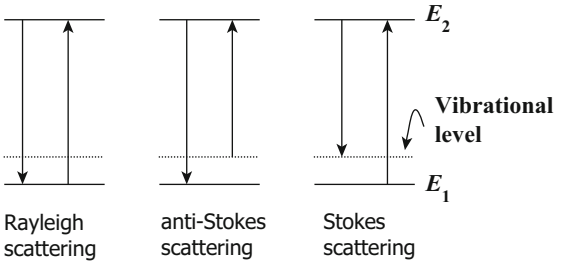

Fig. 18.17 Schematic depiction of various scattering processes within a medium. The incident photon energies are marked by the right-hand-side arrows

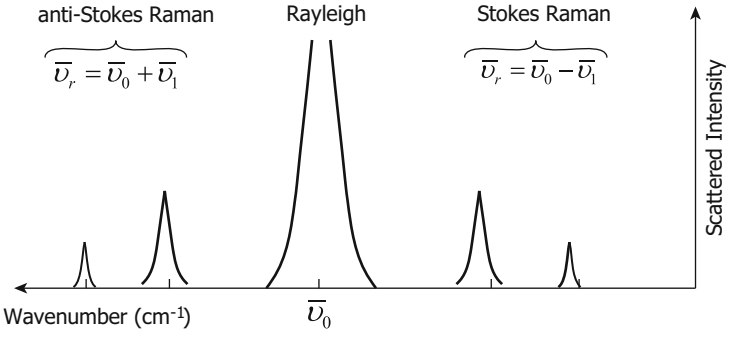

Fig. 18.18 An example of a Raman spectrum representing Rayleigh, Stokes, and anti-Stokes Raman peaks

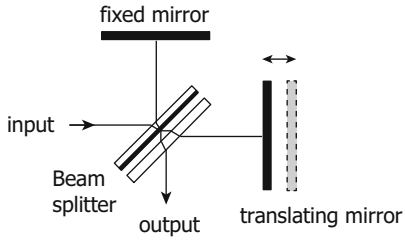

Fig. 18.19 Schematic cross section of a Michelson interferometer

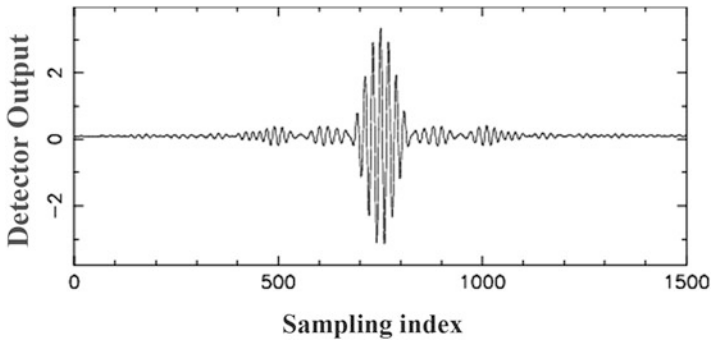

Fig. 18.20 A typical interferogram

Fourier transform). The Michelson interferometer consists of a beam splitter, a fixed mirror, and a mirror that moves back and forth as shown in Fig. 18.19. The input signal is split into two different optical paths, after which they add into the output signal. When the two mirrors are equidistant from the beam splitter, there is constructive interference for a given wavelength, and the output signal is very high. However, when the translating mirror is moving, its separation from the beam splitter varies, and the difference in distance that the two split beams of light have to flow through is called the optical path difference (OPD).

For incident light with a single wavelength, λ, on the input to the beam splitter, the output will have sinusoidal behavior with minima occurring when the OPD is an odd multiple of $\lambda/2$ (destructive interference). For a broadband incident light source, such as the luminescence from a semiconductor, the output intensity is more complicated as shown in Fig. 18.20. When the OPD is equal to zero, all spectral components interfere constructively; therefore, the absolute maximum of the interferogram, also called the center burst, is generated at that position. As the OPD increases, two different wavelengths will not reach a maximum output at the same time, giving us a complex looking oscillatory signal with decreasing amplitude, called the interferogram. It should be noted that when the wavelength of incident light is in the infrared region, this technique is called Fourier transform infrared (FTIR) spectroscopy.

The analog signal of the detector is digitized during the scan using A/D conversion running typically at frequencies up to 120 KHz with a numerical depth of 16 bits. In order to enhance the signal-to-noise ratio, some hundred scans are added

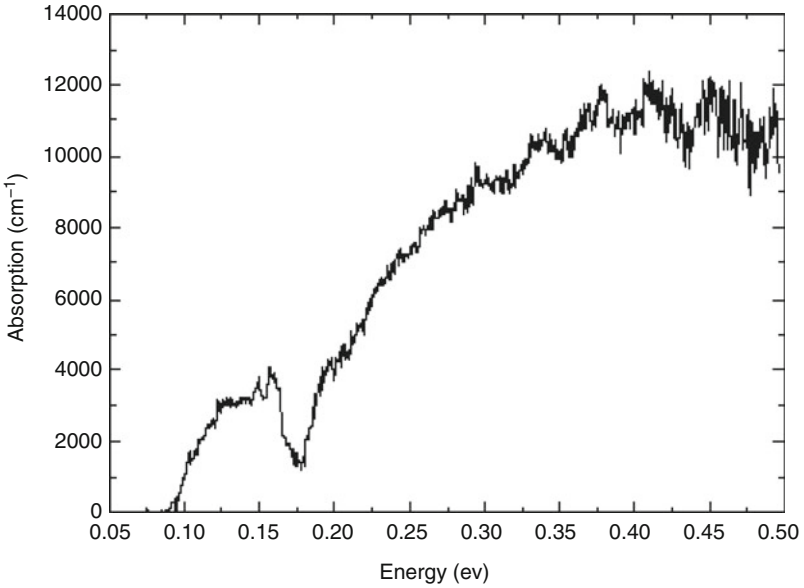

Fig. 18.21 Absorption spectrum for a semiconductor photodetector structure taken by a Fourier transform infrared (FTIR) system

coherently to build up the final interferogram. Once an interferogram is collected, it needs to be translated into an emission spectrum. The process of conversion is through the fast Fourier transform algorithm, which converts the time domain back into the frequency (or wavelength) domain. A typical example of an FTIR spectrum is shown in Fig. 18.21 illustrating the absorption of a semiconductor photodetector structure as a function of energy.

Normally, interferometric spectra are in units of wavenumber. The relationship between wavenumber and wavelength is:

$$\upsilon\left(\mathrm{cm}^{-1}\right) = \frac{10000}{\lambda(\mu m)} \tag{18.13}$$

Therefore, it would be easy to convert wavenumber to other useful units such as wavelength or energy, as is the case in Fig. 18.21.

18.4 Electrical Characterization Techniques

18.4.1 Resistivity

Using sheet resistivity measurement techniques (i.e., the four-point probe technique or the van der Pauw method), one can determine the sheet resistivity, ρ_s (and if the layer thickness is known, the resistivity, ρ), of a semiconductor layer. The

concentration of dopants can also be obtained from sheet resistivity measurements if the value of mobility is known (Eq. 8.8). Usually the carrier mobilities of some of the more established semiconductors, such as silicon, are known, and one can use those values to determine the carrier concentration from resistivity values. However, the type of doping (*n*-type or *p*-type) cannot be deduced from resistivity measurements. This technique is also useful when the carrier concentration varies as a function of depth. In this case, the resistivity will be:

$$\rho(z) = [N(z)e\mu(N)]^{-1} \tag{18.14}$$

where $N(z)$ is the carrier concentration as a function of depth and $\mu(N)$ is the carrier mobility as a function of carrier concentration. The measured sheet resistivity will be the weighted average given by:

$$\rho_s = \left[\int_0^t N(z)e\mu(N)dz\right]^{-1} \tag{18.15}$$

where t is the thickness of the layer.

18.4.2 Hall Effect

With Hall effect measurements, one can determine the concentration as well as the type of the dopants. In addition, the Hall mobility can be deduced from these measurements. Generally Hall effect measurement systems are capable of measuring low carrier concentrations, as low as 10^{14} cm^{-3}. The problems with Hall effect measurements are the rather difficult sample preparation (including contact preparation) and the errors that occur when the substrate is conductive. The reader is referred to Chap. 8 for a complete discussion on the Hall effect.

18.4.3 Capacitance Techniques

In capacitance techniques the charge storage capacity, or capacitance, is measured across a rectifying junction.

Capacitance-voltage (C-V) measurements use a time-varying voltage of variable frequency to determine the majority carrier concentration in the bulk of the device and/or energy levels of interface states that often exist between the surfaces of dissimilar materials. In order to determine the carrier concentration, usually a Schottky diode is built. The diode is then reverse biased and the value of capacitance is measured at each bias point. The carrier concentration can then be calculated as (refer to Chap. 9 for more discussion on junction capacitance):

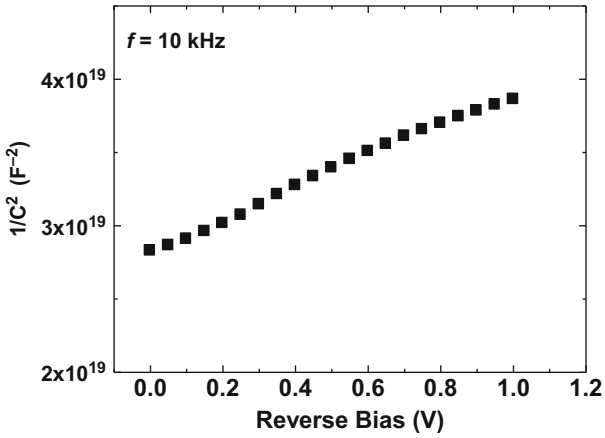

Fig. 18.22 Plot of C^{-2} vs. reverse bias for a p-type GaN sample. The measurements were taken at a frequency of 10 kHz

$$N = \frac{2}{\varepsilon\varepsilon_0 A^2}\left(\frac{1}{d\left(C^{-2}\right)/dV_r}\right) \tag{18.16}$$

where N is the carrier concentration (N_A for p-type, N_D for n-type), ε is the dielectric constant, A is the area of the diode, C is the capacitance, and V_r is the reverse bias. Figure 18.22 shows the plot of $\frac{1}{C^2}$ as a function of reverse bias for a p-type GaN sample. From the slope of the curve and the values of the dielectric constant and the diode area, the majority carrier concentration can be calculated.

Deep-level transient spectroscopy (DLTS) is another capacitance technique that examines the time-dependent flow of charge into and out of localized energy states associated with defects in the semiconductor. DLTS can thus determine many important defect-related properties, such as the nature of defects and their activation energies.

18.4.4 Electrochemical Capacitance-Voltage Profiling

Electrochemical capacitance-voltage (ECV) profiling is a measurement technique that allows one to determine doping level at various depths within a semiconductor structure.

Originally this technique was simply an extension of the CV measurement technique that calculates the average carrier concentration by measuring the capacitance across a Schottky barrier depletion region. In the modified approach, the sample is located inside an electrolyte that produces a well-defined electrochemical dissolution with the semiconductor material. This approach has led to the development of automated ECV profiling systems with nanometer etch depth resolution.

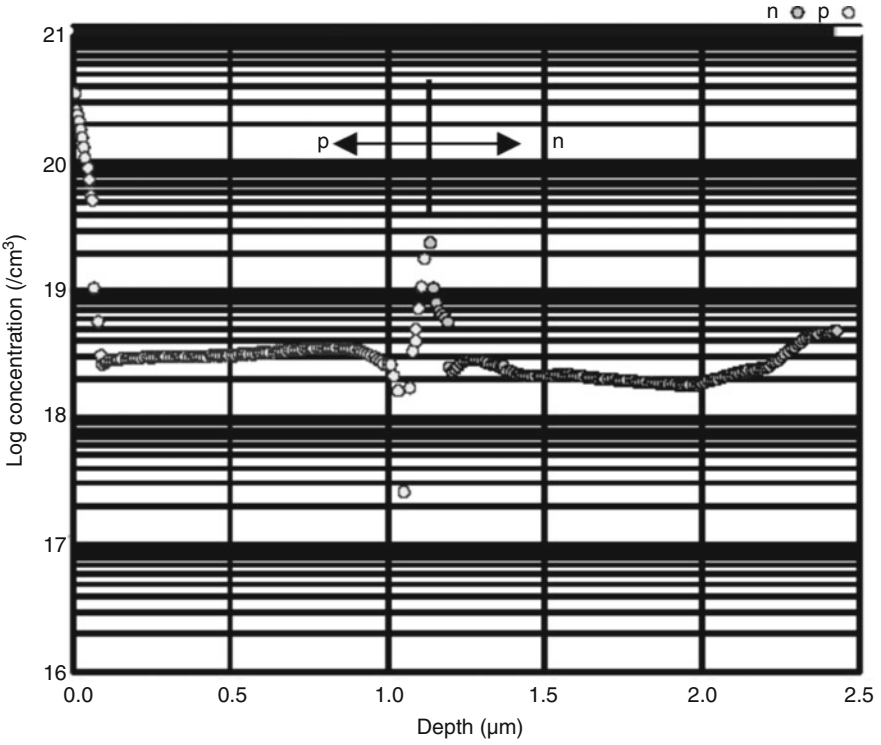

Fig. 18.23 A representative ECV profile showing the concentration of n-type and p-type dopants as a function of depth for a 980 nm laser diode structure

With the ECV profiling, it is not only possible to determine the type of doping (*n*-type, *p*-type) but also the concentration of the dopants in the range of 10^{13}–10^{21} cm^{-3}. An example of an ECV profile is shown in Fig. 18.23

18.5 Summary

In this chapter we discussed several important semiconductor characterization techniques, covering structural, optical, and electrical properties of semiconductors. X-ray diffraction, electron microscopy (SEM and TEM), energy dispersive analysis using X-rays (EDX), Auger electron spectroscopy (AES), secondary-ion mass spectroscopy (SIMS), Rutherford backscattering (RBS), and scanning probe microscopy (SPM) were covered under structural characterization techniques. Optical characterization techniques included photoluminescence spectroscopy (PL), cathodoluminescence spectroscopy (CL), reflectance and absorbance measurements, ellipsometry, Raman spectroscopy, and Fourier transform spectroscopy. Finally, we briefly discussed some of the electrical characterization techniques such as resistivity

measurement, Hall effect measurement, capacitance techniques, and electrochemical capacitance-voltage (ECV) profiling. These characterization techniques are instrumental in understanding the most important properties of various semiconductors as building blocks of many useful electronic and optoelectronic devices.

Problems

1. The incident ion in an RBS measurement setup is $^4He^+$ at $E_0 = 3$ MeV. The angular position of the ion detector, θ, is chosen to be 170°. The backscattered beam from the surface of the sample under test has an energy of 2.5886 MeV. Determine which element of the periodic table the sample under test is made of.
2. In an RBS measurement setup, $^4He^+$ at $E_0 = 2$ MeV is used as incident ions. The scattering angle, θ, is 170 °. The incident ions impinge on a 100 nm thick silicon sample (atomic mass of Si equals 28.08). The majority of He ions penetrate below the surface where they lose their energy at a linear rate of 2 keV/nm. Determine the range of the backscattered energies from the sample ($\Delta E = E_4 - E_1$).

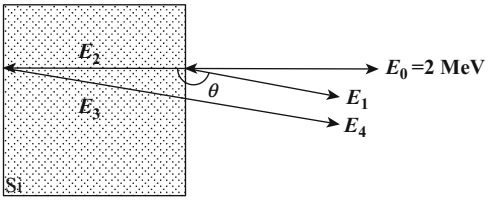

3. Estimate the acceptor concentration of the *p*-type GaN of Fig. 18.22. assuming a diode area of 400 μm × 150 μm and a dielectric constant of $\varepsilon = 10\varepsilon_0$.
4. Based on the SIMS spectrum of Fig. 18.11:
   (a) Estimate the thickness of the oxide layer that has formed on the surface.
   (b) Si is an *n*-type dopant in the GaN material system. What is the doping concentration away from the surface?
5. Based on the photoluminescence spectrum of Fig. 18.15:
   (a) Estimate the Al mole fraction (x) in the $Al_xGa_{1-x}N$ layer. Assume that Vegard's law holds for the calculation of the bandgap energy of the ternary $Al_xGa_{1-x}N$ from the binary compounds GaN ($E_g = 3.4$ eV) and AlN ($E_g = 6$ eV).
   (b) Assuming that the defect-related emission peak arises from the transitions from the valence band to a deep level, estimate how deep into the bandgap this deep level rests with respect to the conduction band edge ($\Delta E = E_C - E_D$).

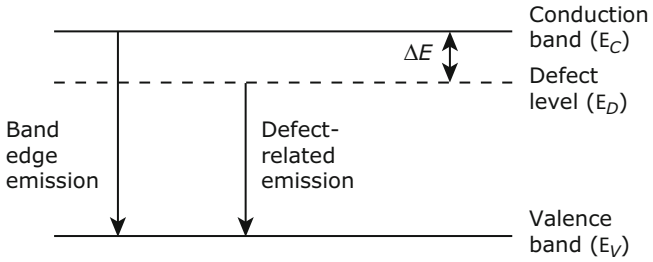

6. In this chapter we introduced four measurement techniques that yield the impurity concentration in semiconductor layers, namely, SIMS, sheet resistivity (SR) measurements, Hall effect measurements, and ECV profiling. Complete the following table to compare these four techniques with respect to the stated application requirements.

Application requirement	SIMS	SR	Hall	ECV
Determination of doping concentration	✓	✓	✓	✓
Determination of doping type (n-type or p-type)				
Determination of the concentration of electrically activated dopants				
Easy sample preparation				
Determination of dopant concentration as a function of depth				
Non-destructive measurement				
Thickness of the layer may be unknown				

7. From the discussion of Rayleigh scattering, we recall that Rayleigh scattering is the elastic scattering of light off molecules that are smaller than the wavelength of that light. The intensity of the scattered light as a function of wavelength is given by:

$$I = I_o\left[\frac{8\pi^4 N\alpha^2}{\lambda^4 R^2}\right]\left(1 + \cos^2\theta\right)$$

Based on this formula, justify why the sky appears blue.

8. Do you think SEM and AFM are competing techniques or complementary techniques? Explain why.
9. Based on the TEM image provided in Fig. 18.7, estimate the lattice mismatch between AlN and sapphire.
10. When an X-ray beam impinges upon a sample, it gets partially transmitted, partially absorbed, and partially scattered (diffracted). The ratio of the intensity of the transmitted beam to that of the incident beam can be expressed as: $\frac{I_T}{I_0} = e^{-\alpha x}$ where α is a constant and x is the thickness of the sample. We know that if the thickness of a sample is doubled, it means that the number of crystallographic planes that cause diffraction from a transmitted beam has been doubled. Based on this, propose a formula that describes the intensity of the diffracted beam versus the incident beam. At what thickness is this intensity maximum? What percentage of light will be transmitted at this optimum thickness?

References

Ohring M (1992) The materials science of thin films. Academic Press, San Diego
Williams DB, Carter CB (1996) Transmission electron microscopy. Plenum Press, New York

Further Reading

Long DA (1977) Raman spectroscopy. McGraw-Hill, New York
Perkowitz S (1993) Optical characterization of semiconductors: infrared, Raman, and photoluminescence spectroscopy. Academic Press, London
Razeghi M (1989) The MOCVD challenge volume 1: a survey of GaInAsP-InP for photonic and electronic applications. Adam Hilger, Bristol
Razeghi M (1995) The MOCVD challenge volume 2: a survey of GaInAsP-GaAs for photonic and electronic device applications. Institute of Physics, Bristol, pp 21–29
Stradling RA, Klipstein PC (1990) Growth and characterization of semiconductors. Adam Hilger, New York
Warren BE (1990) X-ray diffraction. Dover Publications, New York